Scaling of fractal basin boundaries near intermittency transitions to chaos

Bae-Sig Park*
Laboratory for Plasma Research and Department of Physics and Astronomy, University of Maryland, College Park, Maryland 20742

Celso Grebogi
Laboratory for Plasma Research, University of Maryland, College Park, Maryland 20742

Edward Ott
Laboratory for Plasma Research, Department of Physics and Astronomy, and Department of Electrical Engineering, University of Maryland, College Park, Maryland 20742

James A. Yorke
Institute for Physical Science and Technology and Department of Mathematics, University of Maryland, College Park, Maryland 20742
(Received 5 December 1988)

It is the purpose of this paper to point out that the creation of fractal basin boundaries is a characteristic feature accompanying the intermittency transition to chaos. (Here "intermittency" transition is used in the sense of Pomeau and Manneville [Commun. Math. Phys. **74**, 189 (1980)]; viz., a chaotic attractor is created as a periodic orbit becomes unstable.) In particular, we are here concerned with type-I and type-III intermittencies. We examine the scaling of the dimension of basin boundaries near these intermittency transitions. We find, from numerical experiments, that near the transition the dimension scales with a system parameter p according to the power law $d \cong d_0 - k|p - p_I|^\beta$ with $\beta = \frac{1}{2}$, where d_0 is the dimension at the intermittency transition parameter value $p = p_I$ and k is a scaling constant. Furthermore, for type-I intermittency $d_0 < D$, while for type-III intermittency $d_0 = D$, where D is the dimension of the space. Heuristic analytic arguments supporting the above are presented.

I. INTRODUCTION

Intermittency[1] has received considerable attention as one of the typical routes to chaos. Specifically, if we assume that the transition occurs at $p = p_I$ as a parameter p is increased, then for $p < p_I$ the motion is periodic, while for $p > p_I$ it is chaotic. For $p \gtrsim p_I$, the chaotic motion is characterized by long intervals of approximately periodic behavior, similar to that for $p < p_I$, interrupted by short chaotic bursts occurring at irregular times.

In this paper, we are concerned with type-I and type-III intermittencies. Type-I intermittency is associated with a saddle-node bifurcation (tangent bifurcation in one-dimensional maps) and is characterized by a real eigenvalue of the map, linearized about the periodic orbit, crossing the unit circle at $+1$. Type-III intermittency involves an inverted period-doubling bifurcation. For this bifurcation, a real eigenvalue crosses the unit circle at -1.

It is the main purpose of this work to point out that the creation of fractual basin boundaries is a typical feature accompanying type-I and type-III intermittency transitions. That is, if we decrease p through p_I, the attracting motion of the system converts from chaotic to periodic, and there can be fractal basin boundaries in the periodic regime. Thus although the *attracting* chaotic motion is destroyed as p decreases through p_I, chaos is still present and manifests itself in the structure of the basis boundary.

Our main result is that the dimension of the basin boundary near p_I scales as

$$d \cong d_0 - k|p - p_I|^\beta \tag{1a}$$

with $\beta = 1/2$, and d_0 the dimension at $p = p_I$ satisfies

$$d_0 < D \ , \tag{1b}$$

for type-I intermittency, and

$$d_0 = D \ , \tag{1c}$$

for type-III intermittency, where D is the dimension of the phase space.

Sections II and III present numerical experiments supporting the above, while heuristic arguments based on one-dimensional quadratic maps are given in Sec. IV.

Remark: In intermittency transitions, a nonchaotic attractor appears and a chaotic attractor is simultaneously destroyed. After the chaotic attractor is gone the chaos still exists and manifests itself as an unstable (i.e., nonattracting) chaotic set. For the forced damped pendulum equation examples studied in this paper, the closure of the stable manifold of this chaotic set is also the boundary between two different basins of attraction. This situation arises because of the inherent symmetry of the pen-

dulum equation. For nonsymmetric problems, the closure of the stable manifold of the nonattracting chaotic set will typically not be a basin boundary. Nevertheless, the essential situation is the same, and the dimension of the closure of the stable manifold of the unstable chaotic set scales as (1) near the intermittency bifurcation point. (This situation also applies to one-dimensional maps with the added piece of information that the dimension of the chaotic set and its stable manifold are the same.)

II. TYPE-I INTERMITTENCY

As mentioned in the introduction, type-I intermittency occurs when an eigenvalue of the linearized map about a periodic orbit is real and crosses the unit circle at $+1$ as a system parameter is varied. We now discuss two systems which demonstrate the formation of a fractal basin boundary as the system orbit passes from chaotic attractor to periodic attractor via type-I intermittency.

(i) Quadratic map (period-3 window). We consider the one-dimensional quadratic map (the material on the one-dimensional quadratic map has appeared previously in work by McDonald *et al.*[2] and by Napiorkowski[3] and is included here for completeness and as an aid to exposition)

$$x_{n+1}=F(x_n)\equiv A-x_n^2 \ . \tag{2}$$

We focus attention on the period-3 window (Fig. 1) since it is the largest window. The results apply, however, for all windows of Eq. (2). Figure 1 shows the bifurcation diagram exhibiting the period-3 window. As we increase the parameter A, the map experiences a tangent bifurcation at $A_I=1.75$. This bifurcation produces one stable and one unstable period-3 orbit for the F map. However, for the three-times iterated map F^3 each component of the stable period-3 orbit corresponds to a period-1 attractor. Hence the F^3 map has three period-1 attractors for $A \gtrsim A_I$. Each one of these attractors goes through a period-doubling cascade, becomes chaotic at $A \simeq 1.78$, and is destroyed by a crisis[4] at $A \simeq 1.79$. Figure 2 shows

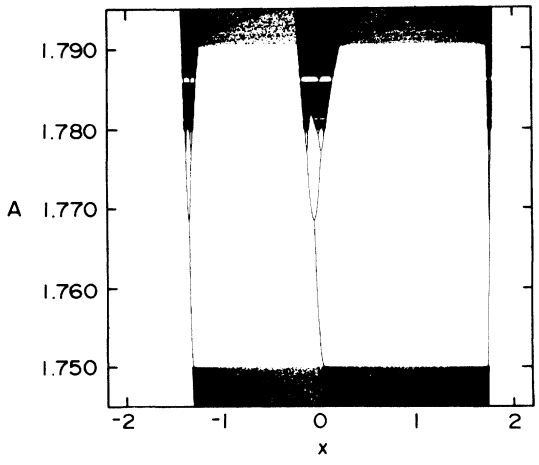

FIG. 1. Bifurcation diagram A vs x for the quadratic map showing the period-3 window.

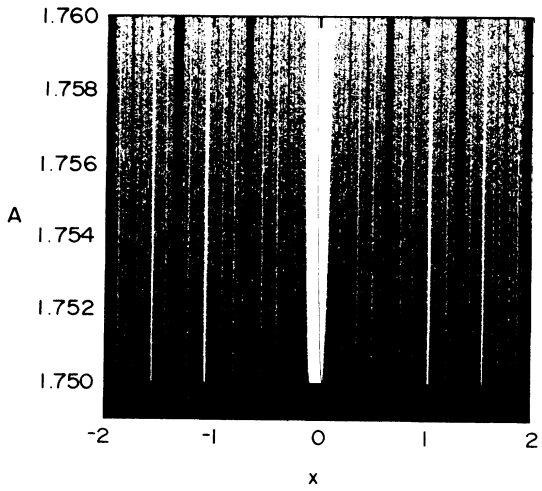

FIG. 2. Basin of attraction for the type-I intermittency in the quadratic map. The middle attractor is in white. The middle period-1 attractor, as a function of the parameter A, is shown by a solid line in the largest gap.

the basin of attraction (in white) for the middle attractor as a function of the parameter A for $1.75 \le A \le 1.76$. To make this picture, we choose 1024 initial conditions for a fixed A value and plot a black dot for the initial conditions which do not go to the middle attractor. We then increase slightly the parameter A and repeat the process. The black region is then the basin of attraction for orbits which go to one of the other two period-1 attractors or to infinity. Note the complicated structure of the boundary separating the white and black regions. Indeed, the basin boundary is fractal.[2] For fixed A, the boundary is a Cantor set.[2,3] We observe that for $A < A_I$ there is only one chaotic attractor.

We desire to establish how the dimension of the fractal basin boundary, shown in Fig. 2, scales with the parameter A as A approaches the intermittency value A_I from above. To determine the dimension of the basin boundary, we numerically evaluate the uncertainty exponent[2,5] α. This exponent measures the scaling of the likelihood for a small perturbation to push a random initial condition into a different basin. Specifically, if ϵ is the size of the error in specifying an initial condition, then the probability of making an error in predicting which attractor the orbit goes to scales as ϵ^α for small ϵ. The exponent α is related[2,5,6] to the dimension d of the basin boundary through

$$\alpha=D-d \ , \tag{3}$$

where D is the dimension of the space.

To determine α for the fractal basin boundary shown in Fig. 2, we fix A and choose a random initial condition x_0. Assuming that there is some uncertainty in the specification of x_0, which is represented by adding a small perturbation to x_0, i.e., $x_0 \to x_0+\epsilon$ and $x_0-\epsilon$, where ϵ is some constant specifying the size of the uncertainty. We then substitute the three initial conditions x_0,

$x_0+\epsilon$, and $x_0-\epsilon$ in the map (2), and iterate (2) to verify which orbits approach the middle attractor (white) and which ones approach infinity or one of the other two attractors (black). If all three final states are not the same, we say that x_0 is uncertain under the perturbation ϵ. We repeat this for a large number of randomly chosen initial conditions until we obtain 3000 uncertain initial conditions. We then obtain the fraction $P(\epsilon; A)$ of initial conditions that is uncertain by dividing 3000 by the total number of randomly chosen initial conditions. Now, change ϵ and repeat the whole procedure for $\epsilon=10^{-m}$, $m=2,3,\ldots,12$. We then plot $P(\epsilon; A)$ versus ϵ on a log-log scale. If the data are well-fit by a straight line, a power law dependence of P on ϵ is indicated, where the exponent $\alpha(A)$ is given by the slope of the line,[2,5,6]

$$P(\epsilon; A)\sim\epsilon^{\alpha(A)}, \tag{4}$$

for small ϵ [with $\alpha(A)\leq 1$]. Finally, we change A in the range $A_I+10^{-4}\leq A\leq A_I+10^{-2}$ and plot $\alpha(A)$ versus A.

We find that our experiments confirm our analytic arguments in Sec. IV, namely, that the uncertainty exponent α displays the following scaling law:

$$\alpha(A)=\alpha_0+k|A-A_I|^{\beta}, \tag{5}$$

where β is a universal exponent for the scaling of fractal basin boundaries near type-I intermittency, and α_0 and k are constants which depend on the periodic window in consideration.[3] Since from Eq. (3) $d=D-\alpha$, the dimension of the basin boundary scales, with the parameter A, as given by Eq. (1a), where p is substituted by the parameter A (and p_I by A_I) and $d_0=D-\alpha_0$. In Fig. 3 we make a log-log plot of $|d-d_0|/k$ versus $|A-A_I|$. We use a simplex algorithm to make three parameter least-squares fit of the line shown in Fig. 3 to Eq. (1). We find that as A approaches A_I from above, the dimension converges to the value $d(A_I)\equiv d_0=0.971\pm0.002$, which is less than one and thus verifying Eq. (1b). The exponent in Eq. (1a) is found to be $\beta=0.50\pm0.02$ and the constant $k=0.54\pm0.01$.

(ii) Forced damped pendulum. The second nonlinear system for which we investigate Eqs. (1a) and (1b) is the forced damped pendulum equation,

$$\ddot{\theta}+\nu\dot{\theta}+\omega_0^2\sin\theta=f\cos\omega t, \tag{6}$$

where ν is the damping parameter, $\omega_0^2\sin\theta$ is the gravitational restoring torque, and $f\cos\omega t$ is the driving torque. We set $\omega=1$ in this work. Several physical systems (Josephson junction,[7-9] phase-locked loops,[7] etc.) can be modeled by Eq. (6).

The integration of Eq. (6) for one driving period (from $t=0$ to $t=2\pi$) defines a Poincaré map. In this case, a period 2π attractor, which has the same period as the sinusoidal driving torque, appears as a fixed point in the Poincaré section.

The forced damped pendulum equation has a natural symmetry[9,10] with respect to the transformation $(\theta\rightarrow-\theta, t\rightarrow t+\pi)$, i.e., if $(\theta(t),\dot{\theta}(t))$ is a solution of Eq. (6), then so is $(-\theta(t+\pi),-\dot{\theta}(t+\pi))$. As a consequence, nonsymmetric asymptotic solutions always occur in pairs.

For $\nu=0.2$ and $\omega_0^2=1.05$, we identify type-I intermittency as we increase f. In Fig. 4, we show a bifurcation diagram where we plot θ (measured at times $t=2n\pi$, $n=0,1,\ldots$) versus f for f very close to the inverse saddle-node bifurcation value $f_I\simeq 2.172\,083\,5$. In this diagram, the solid lines denote an attractor while the solid lines with dots denote a period-2 unstable periodic orbit. The period-1 attractor experiences a period-doubling bifurcation at $f\simeq 2.166\,86$. This is a nonsymmetric attractor,[10] therefore, there also exists another attractor which is the image under $\theta\rightarrow-\theta$, $t\rightarrow t+\pi$ of the one depicted in Fig. 4, and this second attractor has precisely the same bifurcation value $f=f_I$. For $f>f_I$ the system has only one (symmetric) chaotic attractor. In Fig. 5, we show the

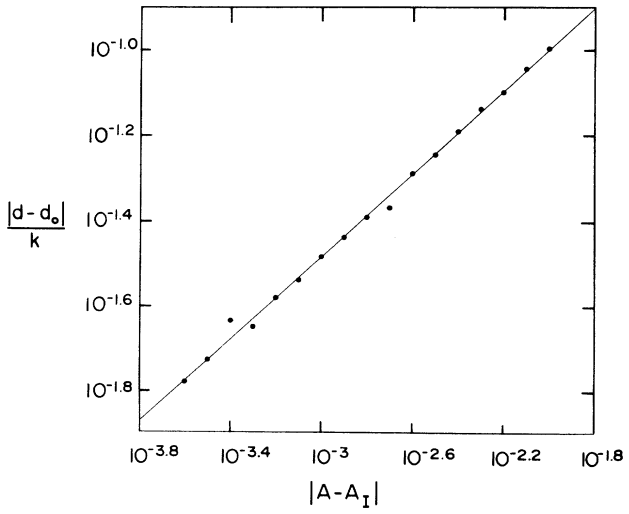

FIG. 3. The log-log plot of $|d-d_0|/k$ vs $|A-A_I|$.

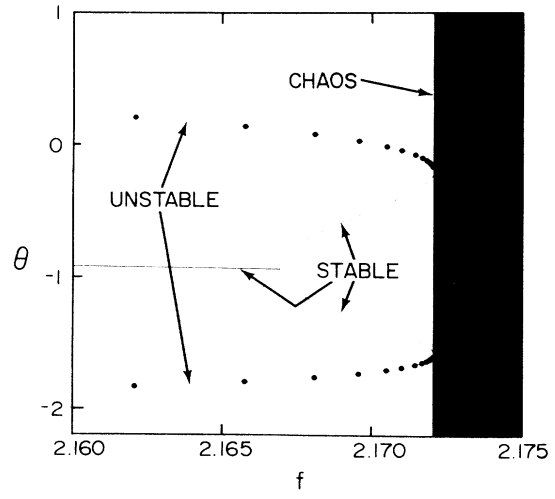

FIG. 4. Bifurcation diagram where we plot θ vs f for f near the bifurcation parameter value f_I for the inverse saddle-node bifurcation.

basins of attraction for the two period-1 attractors when $f=2.1645$. The coordinates of the attractor in the white basin are $(\theta,\dot{\theta})=(-0.928\,230, 2.129\,915)$ and the coordinates of the attractor in the black basin are $(\theta,\dot{\theta})=(-0.827\,191, -0.461\,160)$. The basins of attraction in Fig. 5 are computed for a 1024×1024 grid of initial conditions $(\theta_0,\dot{\theta}_0)$ spanning $-\pi\le\theta_0\le\pi$ and $-5.0\le\dot{\theta}\le5.0$. for each initial condition, we integrate Eq. (4) until the solution becomes sufficiently close to one of the attractors. If an initial condition is asymptotic to the attractor at $(\theta,\dot{\theta})=(-0.827\,191, -0.461\,160)$, a black dot is plotted corresponding to that initial condition. If the orbit approaches instead the other attractor, no dot is plotted. Note that the white and black basins of attraction exhibit a fine-scale structure indicative of a fractal basin boundary.

To determine how the dimension of the basin boundary scales as the parameter value approaches f_I from below, we use a procedure similar to the one described in (i) of Sec. II for the quadratic map. Namely, we evaluate the uncertainty exponent $\alpha(f)$ for various values of f and from it we derive $d(f)=D-\alpha(f)$. The only difference in the procedure to evaluate $\alpha(f)$ is that we now have a two-dimensional phase space $(\theta,\dot{\theta})$ and the initial conditions are chosen randomly in this space. We then add a small perturbation $+\epsilon$ and $-\epsilon$ to one of the coordinates or to some combination of both. We measure $\alpha(f)$ for f in the range $f_I-10^{-2}<f<f_I-10^{-4}$.

Consistent with Eq. (1a) a straight line provides a reasonable fit to the data. Figure 6 shows a log-log plot of $|d-d_0|/k$ versus $|f-f_I|$. By using the Simplex algorithm, we find that d converges to $d_0=1.960\pm0.002$ [consistent with Eq. (1b)] as f approaches f_I, $d=0.20\pm0.01$, and the slope $\beta=0.50\pm0.02$.

For the pendulum as well as for the quadratic map, the dimension of the fractal basin boundary for type-I intermittency scales with the parameter according to Eq. (1a), where the scaling exponent is $\beta=\frac{1}{2}$ and the dimension of the boundary is less than the dimension of the space at intermittency, i.e., $d_0<D$ for $p=p_I$ [Eq. (1b)].

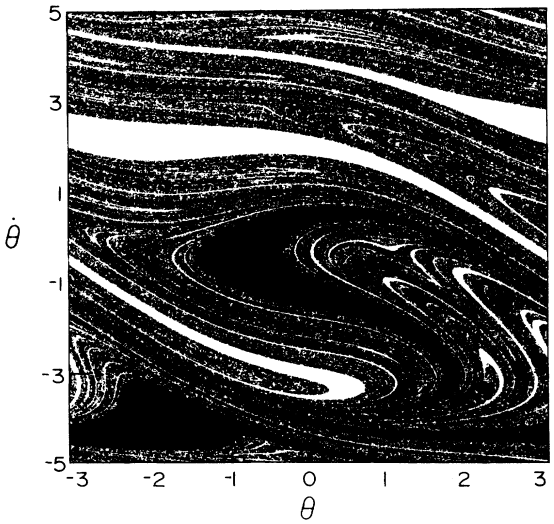

FIG. 5. Basins of attraction for the forced damped pendulum near the type-I intermittency for $\nu=0.2$, $\omega_0^2=1.05$, and $f=2.1645$.

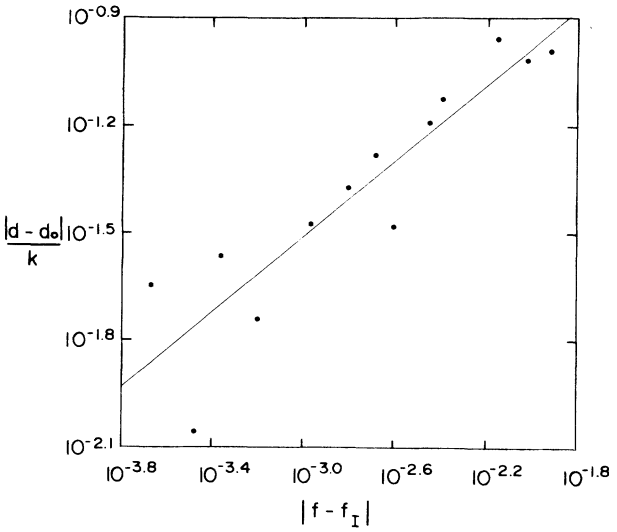

FIG. 6. Log-log plot of $|d-d_0|/k$ vs $|f-f_I|$ for type-I intermittency in the pendulum.

III. TYPE-III INTERMITTENCY

Type-III intermittency involves an inverted period-doubling bifurcation. In this bifurcation the nonlinear system has a stable periodic orbit and a corresponding unstable orbit with twice its period. Then, as the parameter increases, the unstable orbit collapses onto the attractor, and the attractor loses its stability as its associated eigenvalue decreases through -1. For parameter values above this bifurcation, the periodic attractor becomes an unstable orbit and the attractor is chaotic. However, for parameter values close to the bifurcation but in the chaotic side, the unstable orbit controls the dynamics. That is, an orbit injected close to the unstable periodic orbit takes a relatively long time to leave that neighborhood and, in the meantime, executes motion that is approximately periodic.

Inverted period doubling cannot occur for the one-dimensional quadratic map (because it has negative Schwartzian derivative), but it does occur in Eq. (6) for the forced damped pendulum. In Fig. 7, we show a type-III intermittency transition bifurcation diagram for the pendulum, Eq. (6), where we plot $\dot{\theta}$ versus f. The other parameters are set at $\nu=0.1$ and $\omega_0^2=0.8$. This bifurcation diagram shows an inverted period doubling. The solid line denotes a period-1 attractor of the Poincaré map, while the solid line with dots indicates a period-2 unstable orbit. The bifurcation value of the parameter is $f_{III}\simeq2.054\,938$. As we discussed in Sec. II, symmetry considerations require that nonsymmetric attractors come in pairs. Therefore there is another period-1 attractor for $f<f_{III}$, which gives a bifurcation diagram similar

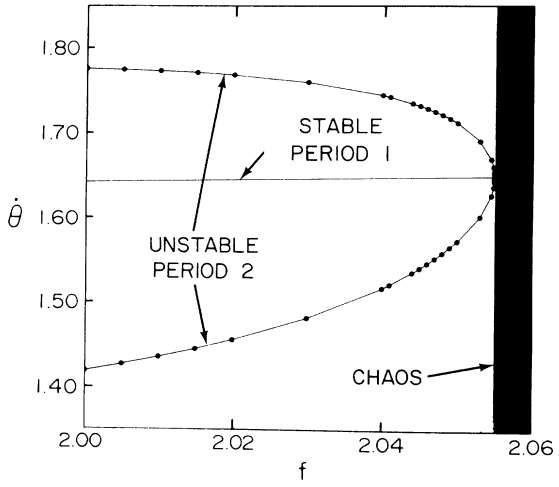

FIG. 7. Bifurcation diagram $\dot{\theta}$ vs f near the bifurcation parameter $f_{\rm III}$ for the inverted period-doubling bifurcation.

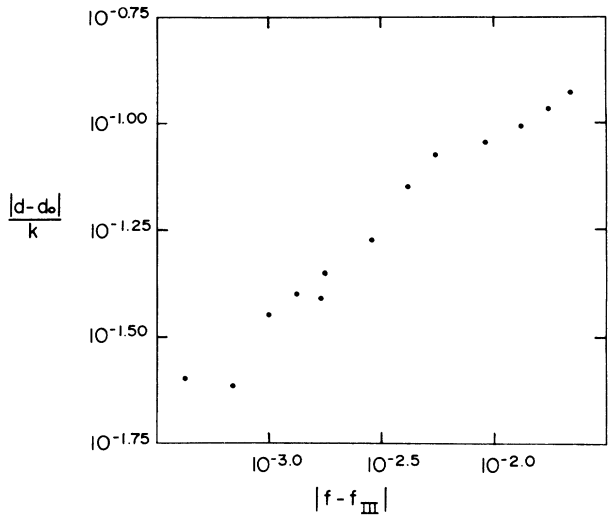

FIG. 9. Log-log plot of $|d-d_0|/k$ vs $|f-f_{\rm III}|$ for type-III intermittency in the pendulum.

to the one shown in Fig. 7 with the bifurcation at precisely the same point $f=f_{\rm III}$. However, for $f>f_{\rm III}$, there is only one chaotic attractor which is symmetric.

Figure 8 shows the basins of attraction for the two period-1 attractors for $f=2.04$. The attractor corresponding to the white basin has coordinates $(\theta,\dot{\theta})=(-0.785\,172, 1.646\,778)$ and to the black basin $(\theta,\dot{\theta})=(-0.657\,705, -0.903\,553)$. To determine the dimension of the fractal basin boundary near the type-III intermittency, we evaluate the uncertainty exponent $\alpha(f)$ in the range $f_{\rm III}-10^{-1.5}<f<f_{\rm III}-10^{-3.5}$. In evaluating $\alpha(f)$ we follow the same numerical procedure outlined in Sec. II. We find that the dimension for the type-III intermittency also obeys Eq. (1) [where p (and $p_{\rm I}$) is replaced by f (and $f_{\rm III}$)]. In Fig. 9, we plot $|d-d_0|/k$ versus $|f-f_{\rm III}|$. By employing the same Simplex algorithm as before, we find $d_0=2.000\pm0.001$, $k=0.095\pm0.006$, and $\beta=0.51\pm0.03$. This result is consistent with Eqs. (1a) and (1c). In particular, according to Eq. (1c), as f approaches $f_{\rm III}$, the dimension of the basin boundary approaches that of the space, i.e., $d_0=D$.

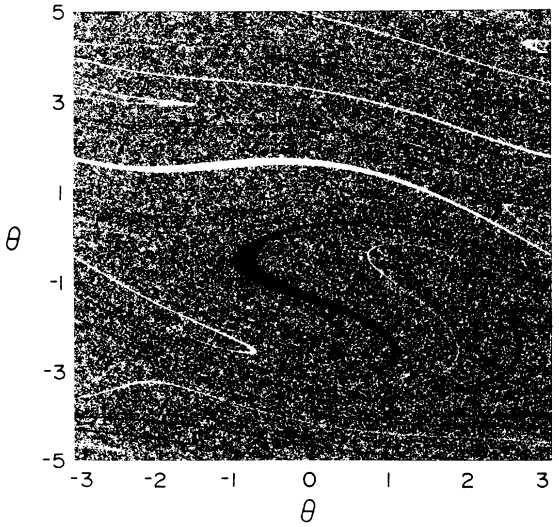

FIG. 8. Basins of attraction for the forced damped pendulum near the type-III intermittency for $\nu=0.1$, $\omega_0^2=0.8$, and $f=2.04$.

IV. DISCUSSION

Numerically we found that for type-I intermittency $d_0<D$ at $p=p_{\rm I}$ ($d_0\simeq0.971$ for the logistic map and $d_0=1.960$ for the forced damped pendulum) and for the type-III intermittency $d_0=D$ ($d_0\simeq2.000$ for the forced damped pendulum). In the following, we examine these results in terms of one-dimensional maps.

The geometric structure of a one-dimensional map exhibiting type-I intermittency is shown in Fig. 10. In Fig. 10(a) we show the map for $p<p_{\rm I}$. In this case, the map has two fixed points, the one labeled U is unstable and the other labeled A is stable. Construct the interval (U', U), where U' is the preiterate of U. Observe that this whole interval is asymptotic to the attractor A. We also suppose that the neighborhoods to the right of U and to the left of U are attracted to some other attractor. Then, the basin of attraction of the attractor A is made up of the

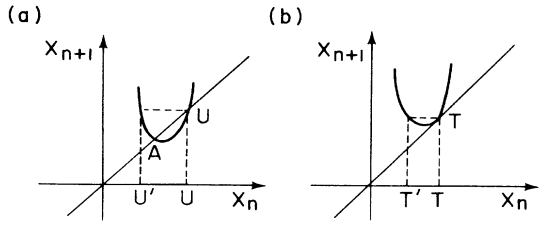

FIG. 10. Type-I intermittency. (a) $p<p_{\rm I}$. (b) $p=p_{\rm I}$.

interval (U',U) and all the preiterates of the interval (U',U). As we increase the parameter p to its value p_I at the tangent bifurcation, the fixed points A and U coalesce to the tangential point T, as shown in Fig. 10(b). Observe that T is repelling on its right but attracting on the interval (T',T), where T' is the preiterate of T. Hence, at $p=p_I$, the basin of attraction of T has finite area and is made up of the interval (T',T) and all its preiterates.

We can think of the fractal basin boundary as resulting from the construction of a Cantor set. Essentially, we are removing open sets (T',T) and all its preiterates. We also remove open sets corresponding to the other basin of attraction. What remains is a Cantor set of zero Lebesgue measure, meaning that $d_0<D$. This occurs for all values of the parameter p for type-I intermittency.

For the one-dimensional quadratic map shown in Fig. 2, (U',U) corresponds to the middle white strip. Observe that for $A=A_I=1.75$, the width of the white band is still finite, and it corresponds to the interval (T',T). Similarly, for the forced damped pendulum, the width of the white, or black, region, where the attractor is located, does not shrink to zero as $f\to f_I$.

Type-III intermittency is exhibited by a one-dimensional map having the structure shown in Fig. 11. For $P<p_{III}$ there is one attractor A and two saddles U_1 and U_2 as shown in Fig. 11(a). The interval (U_1,U_2) is attracted to A. We can assume that there is another attractor having a different basin to the left of U_1 and to the right of U_2. As the parameter p increases and approaches p_{III}, the interval (U_1,U_2) shrinks to zero, as shown in Fig. 11(b). Therefore the region of the fractal basin boundary covers the whole space at $p=p_{III}$. It is like constructing a Cantor set where the length of the removed open sets shrink to zero. Then, one is left with a

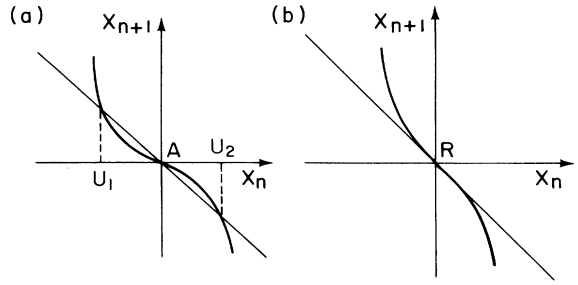

FIG. 11. Type-III intermittency. (a) $p<p_{III}$. (b) $p=p_{III}$.

segment. This is what occurs in the forced damped pendulum example of Sec. III. The width of the white, or black, strip in the neighborhood of the attractor shrinks to zero as $f\to f_{III}$ and $d_0=2.0$. Therefore as the parameter approaches the type-III bifurcation value, the dimension of the basin boundary increases to the dimension of the space D.

The square-root scaling of the dimension with parameter can also be justified in terms of one-dimensional maps. In Fig. 10, the width of the interval (U',U) decreases toward $|T-T'|$ with a square-root dependence on $|p-p_I|$ as $p\to p_I$ from above, $(U-U')-(T-T')\sim|p-p_I|^{1/2}$ (see Fig. 4). The same parameter dependence occurs for the type-III intermittency, $U_2-U_1\sim|p-p_{III}|^{1/2}$ (see Fig. 7).

ACKNOWLEDGMENTS

This work was supported by the U.S. Department of Energy (Basic Energy Sciences).

*Permanent address: Department of Physics, New Mexico State University, Las Cruces, NM 88005.

[1]Y. Pomeau and P. Manneville, Commun. Math. Phys. **74**, 189 (1980).

[2]S. W. McDonald, C. Grebogi, E. Ott, and J. A. Yorke, Physica D **17**, 125 (1985).

[3]M. Napiórkowski, Phys. Rev. A **33**, 4423 (1986).

[4]C. Grebogi, E. Ott, and J. A. Yorke, Physica D **7**, 181 (1983).

[5]C. Grebogi, S. W. McDonald, E. Ott, and J. A. Yorke, Phys. Lett. **99A**, 415 (1983).

[6]C. Grebogi, E. Ott, J. A. Yorke, and H. E. Nusse, Ann. N. Y. Acad. Sci. **497**, 117 (1987).

[7]D. d'Humières, M. R. Beasley, B. A. Huberman, and A. Libchaber, Phys. Rev. A **26**, 3483 (1982).

[8]R. F. Miracky, M. H. Devoret, and J. Clark, Phys. Rev. A **31**, 2509 (1985).

[9]M. Iansiti, Q. Hu, R. M. Westervelt, and M. Tinkham, Phys. Rev. Lett. **55**, 746 (1985).

[10]J. W. Swift and K. Wiesenfeld, Phys. Rev. Lett. **52**, 705 (1984).